Structural Characterization And Exafs Wavelet Analysis Of Yb Doped Zno By Wet Chemistry Route

Eugenio H. Otal, Elsa Sileo, Myriam Aguirre, Ismael O. Fabregas, Manuela Kim

PII: S0925-8388(14)02359-7
DOI: http://dx.doi.org/10.1016/j.jallcom.2014.09.186
Reference: JALCOM 32303

To appear in: *Journal of Alloys and Compounds*

Received Date: 13 July 2014
Revised Date: 19 September 2014
Accepted Date: 23 September 2014

Please cite this article as: E.H. Otal, E. Sileo, M. Aguirre, I.O. Fabregas, M. Kim, Structural Characterization And Exafs Wavelet Analysis Of Yb Doped Zno By Wet Chemistry Route, *Journal of Alloys and Compounds* (2014), doi: http://dx.doi.org/10.1016/j.jallcom.2014.09.186

Structural characterization and EXAFS wavelet analysis of Yb doped ZnO by wet chemistry route.

Eugenio H. Otal [*a, b], Elsa Sileo[c], Myriam Aguirre[d,e,] Ismael O. Fabregas[a] and Manuela Kim[a, b]

[a] Division of Porous Materials, UNIDEF, CITEDEF, CONICET, S. J. B de la Salle 4397, Villa Martelli (B1603ALO), Buenos Aires, Argentina.

[b] Laboratory for Materials Science and Technology, FRSC-UTN, Av. Inmigrantes 555, Río Gallegos (9400), Argentina.

[c] INQUIMAE, Departamento de Química Inorgánica, Analítica y Química Física, Facultad de Ciencias Exactas y Naturales, Universidad de Buenos Aires, Argentina

[d] Dept. of Physics Condensed Matter, University of Zaragoza, Spain

[e] Laboratory of Advanced Microscopy (LMA), Institute of Nanoscience of Aragón (INA), University of Zaragoza, Spain

ABSTRACT.

Lanthanides doped ZnO is an interesting material for optical and electrical applications. The wide band gap of this semiconductor makes it transparent in the visible range (E_{gap} = 3.2eV), allowing a sharp emission from intra shell transition from the lanthanides. From the electrical side, ZnO is a widely used material in varistors and its electrical properties can be tailored by the inclusion of lanthanides. Both applications are influenced by the location of the lanthanides, grain boundaries or lattice inclusion. Yb doped ZnO samples obtained by wet chemistry route were annealed at different temperatures and characterized by Transmission Electron Microscopy (TEM), X-Ray Diffraction (XRD), Rietveld refinement of XRD data, and X-ray Absorption Fine Structure (XAFS). These techniques allowed to follow the changes occurred in the matrix and the Yb environment. The use of the Cauchy continuous wavelet transform allowed identifying a second coordination shell composed of Zn atoms, supporting the observations from XRD Rietveld refinement and XAFS fittings. The information obtained confirmed the incorporation of Yb in Oh sites of the wurtzite structure without Yb_2O_3 clustering in the lattice.

KEYWORDS

Semiconductor, Precipitation, Optical Materials, Lanthanides doping, EXAFS, Wavelet analysis

1. INTRODUCTION

ZnO is an interesting material due to its structural, electrical and optical properties. The structural properties are related to its wurtzite structure (space group $P6_3mc$), that allows obtaining varied morphologies of the oxide: colloidal nanoparticles[1], nanostructured colloids[2], nanorods[3-6], nanowires[7-9], and tetrapods[10], thin films[11], among another complex nanostructures[12-14]. To obtain these morphologies several methods as: thermal evaporation[7, 10], [13], laser ablation[4], hydrothermal synthesis[3, 6], [8], [14], forced hydrolysis[2, 12], precipitation[1] and electro-deposition[5],[15], are implemented.

The nonlinear current-voltage (I-V) properties of ZnO, are known since the ´50[16], however it was not until the ’70s, when Matsuoka[17] rediscovered its electrical properties settling the basis for the implementation of ZnO in varistors. In spite of the origin of the nonlinear I-V behavior that is not completely understood, it was reported that ions segregation at the interfaces has a great influence in this phenomena. Just as an example, Sato et al. showed that in the ZnO:Pr system, the Pr atoms are located at the grain boundaries[18], and Jiang et al. demonstrated that for ZnO:Yb, the Yb presence induces oxygen rich zones by means of a detailed HRTEM-EELS analysis[19].

The good optical properties of ZnO have intensified the interest in this material for applications in hybrid light-emitting diodes [20-22], and its doping with lanthanides (Ln) as activators [23-25] has a potential use in flat displays. One drawback for these last applications is that the energy transfer from the host to the Ln ion is not efficient enough, making them not suitable to be used in devices[26]. The origin of this observation may be attributed to the fact that Ln ions occupy an interstitial site in the lattice[27].

To have a deeper knowledge on the electrical and optical properties of Ln doped ZnO, it is important to determine whether the Ln ions are located into the structural framework, or whether

they are segregated in the grain boundaries[28]. In this work, we present a soft chemistry route for the synthesis of ZnO:Yb and its characterization based on Transmission Electron Microscopy (TEM), X-Ray Diffraction (XRD), Rietveld refinement of XRD data and X-Ray Absorption Fine Structure Spectroscopy (XAFS).

The x-ray diffraction technique (XRD) provides information of the host matrix. Differences in the cell parameters of pure and doped samples, treated at different temperatures, supplied experimental evidence of the incorporation of Yb atoms in the ZnO lattice. On the other hand, the X-Ray absorption measurements (X-ray Absorption Near Edge Spectroscopy and XANES, and Extended X-ray Absorption Fine Structure, EXAFS) are specific to the Yb atoms environment providing structural information of the changes taking place in samples with different thermal treatment.

Taking into account the EXAFS equation[29, 30]:

$$X(k) \approx \sum_j S_i(k) \frac{N_j}{kR_j^2} \left| f_i(k,\pi) \right| e^{-\frac{2R_j}{\lambda_j(k)}} e^{-2\sigma_j^2 k^2} \sin(2kR_j + \sum \phi_{ij}(k))$$

Where S_i is the amplitude reduction factor for the total central atom loss, N_j and R_j are the number of neighbor atoms and the distance of each one from the central atom, $\left| f_i(k,\pi) \right|$ is the effective curved-wave backscattering amplitude function, σ_j^2 is the Debye-Waller term, λ_j is the photoelectron mean-free path, and $\Sigma\, \phi_{ij}(k)$ is the sum over all the phase shifts.

Based on this, the identity of the backscattering atoms can be determined by the backscattering function. Wavelet analysis allows improving the data analysis due to the possibility to observe all the EXAFS contributions simultaneously, obtaining a tridimensional representation of k (reciprocal) and R (real) space.

Several reports can be found about the fundamental of wavelet analysis[31-33] and its implementation[30],[34],[35]. In our case, we applied the Continuous Cauchy Wavelet Analysis (CCWT) to the EXAFS spectra which allows determining the identity of the atoms in noisy signals[30],[36].

The correlation of the experimental results provided a conclusive structural evidence of the Ln incorporation in the structural framework and a range of temperature for thermal annealing to obtain ZnO:Yb without phase segregation.

2. EXPERIMENTAL SECTION

Zinc acetate dihydrated ($Zn(AcO)_2.2H_2O$, (puriss. - Sigma-Aldrich) (ZAD), ytterbium acetate octahydrated ($Yb(AcO)_3.8H_2O$) (99.9% - Sigma-Aldrich), potassium hydroxide (KOH) (p.a. - Merck), absolute ethanol (EtOH) (p.a. - Merck), dimethylformamide (DMF) (p.a. - J. T. Baker) and hexane (p.a - Riedel-de Haen) were used without further purification. Hydration water from lanthanides acetates were quantified by thermogravimetric analysis up to 1000°C for full conversion into sesquioxides.

The synthetic path is a modification of that reported by Schwartz et al. [1]. In our route colloidal nanocrystalline ZnO was synthesized at room temperature by the addition of an ethanolic solution of KOH to ZAD dissolved in DMF. Ethanolic solution was prepared dissolving 0.93 g of KOH in 30 mL of EtOH by sonication during 15 min to obtain a clear solution (0.552 mol/L). The DMF solution was obtained by simply stirring 1.99 g ZAD (9.1 mmol) in 90 mL dimetilformamide (0.101 mol/L). The basic solution was added drop wise at approximately 2 mL/min to the DMF solution under constant stirring, and precipitation was achieved by addition of ethyl acetate. Yterbium-doped ZnO was prepared by using a DMF solution that contained $Yb(AcO)_3 \cdot 8H_2O$ (0.09 mmoles) and $Zn(AcO)_2 \cdot 2H_2O$ (9.0 mmol). To purify the obtained solid, the nanoparticles were re-

suspended in ethanol and precipitated with hexane. The final solids were dried at 70°C overnight, and thermally treated at 500, 600, 700, 800, 900 and 1000°C for 1 hour. Samples were named from ZnO:Yb-070 to ZnO:Yb-1000, respectively.

XRD was performed in a PW 3710 Phillips diffractometer using Cu K_α radiation ($K_{\alpha 1}$ = 1.54056Å), and a Bragg-Brentano configuration. XRD patterns were obtained in the range 20-100° using a 0.02° scanning step and a 10 s step time. The instrumental contribution to the diffraction peak broadening was corrected using a LaB_6 standard (NIST SRM 660). Rietveld refinement was performed with GSAS/EXPGUI[37]. The background was fitted by a Shifted Chebyshev function and the peak shape by the function proposed by Stephens[38].

Samples without thermal treatment were dispersed in ethanol to perform TEM observation. A few drops of the suspension were deposited in a Cu-carbon coated grid. The TEM analysis was performed in a Philips CM30 operated at 300 kV.

XAFS measurements were performed in the D08B-XAFS2 beam line of the Brazilian Synchrotron Light Laboratory (LNLS). The spectra were obtained at room temperature in fluorescence mode with a 15 elements Ge detector. The incident beam at the sample (I_0) and the reference (I_1/I_2) were recorded with ionization chambers as detectors. Samples were diluted with BN and placed at 45° respect to the beam (fluorescence configuration). The copper K-edge (8979eV) was used for energy calibration, measuring the spectra of a copper film together with every sample. The LNLS D08B-XAFS2 beam line is optimized for XAFS spectroscopy in the 4-18 keV energy range. The beam line optics consists of a cylindrical Rh-coated Si mirror for vertical collimation, a Si 111 double crystal monochromator, followed by a ULE Rh-coated bendable toroidal mirror for horizontal and vertical focusing. The beam line yields a flux of $2x10^{10}$ photons/sec/100 miliamps onto a $1mm^2$ beamspot, with an (instrumental) energy resolution of 1.2 eV at 7 keV. The energy

and average current of the storage ring were 1.37 GeV and 140 mA, respectively. Calculations were made assuming that the first coordination shell was formed entirely by oxygen atoms. The inelastic loss scattering factors, S_0^2, were determined from Yb_2O_3 standard (S_0^2 = 0.86). Data reduction and fitting was performed with ATHENA and ARTHEMIS codes respectively[39]. The k-weighted EXAFS signal, $k\chi(k)$, was filtered by a Kaiser-Bessel function with dk = 1.0 and dR = 0.0, and used in the range 3.5-9.4. The fitting was performed in the R range 0.9-2.7. The used k weight for the first shell was 3. CCWT was performed following Muñoz et al[30],[36]. FEFF paths were simulated with ARTHEMIS code.

3. RESULTS AND DISCUSSION

3.1 TEM analysis

The HRTEM images (Figure 1) shows the good crystallinity of the agglomerated nanoparticles. This is corroborated by FFT (Fast Fourier Transform) that shows a sharp ring pattern. The size distribution of nanoparticles ranges within a 4-8 nm interval.

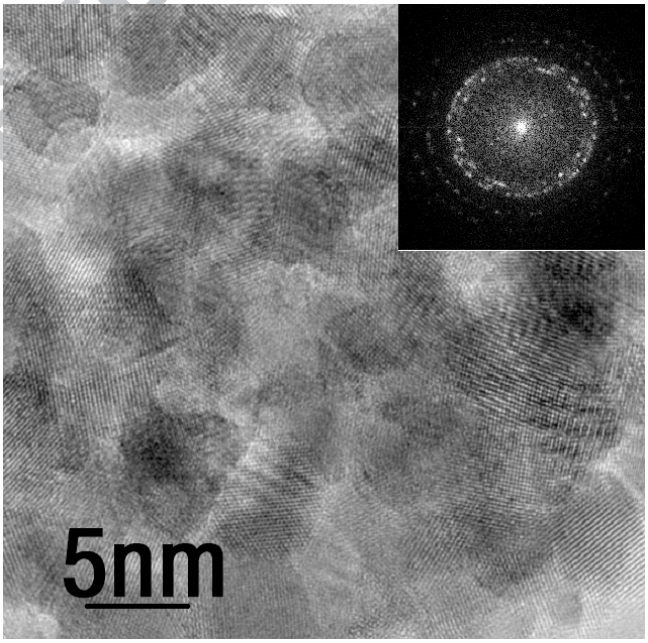

Figure 1 - TEM micrograph of sample ZnO:Yb-070. The inset shows the Fast Fourier Transform and indicates no preferential orientation and the good crystallinity of the nanoparticles.

Nanoparticles agglomeration did not show any preferential orientation in spite of some specific orientations such as [001], [101] and [110] zone axis that can be observed in the nanoparticles at the edge of the colloidal particles.

3.2 XRD analysis

The ZnO:Yb-070 sample diffractogram is shown in Figure 2. The peaks observed correspond to the ZnO wurtzite phase (Space Group: $P6_3mc$ (186) PDF 01-079-2205) with a peak broadening due to the small particle size. No evidence of impurities or other phases was found. Crystal size, obtained by applying the Scherrer equation indicates a mean coherence path dimension of about 10 nm. No anisotropic growth was detected by determining the mean coherence path dimension in the three principal growth directions (reflections 100, 002 and 101).

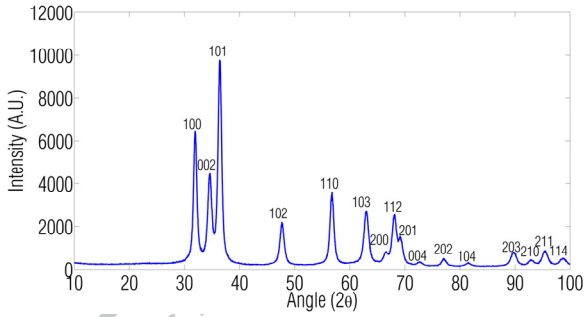

Figure 2 - XRD pattern of sample ZnO:Yb-070.

The cell parameter evolution, obtained by applying the Rietveld refinement method, was used to determine the lanthanide incorporation in the ZnO host. The goodness of the fittings can be found in table 1 and 2 (see Supporting Information).

Figure 3 shows the variations in cell volume of ZnO and ZnO:Yb-070 samples when heated at 500, 600, 700, 800, 900 and at 1000 °C. Both series follow a similar trend, a decrease in cell volume with increasing annealing temperature. This behavior may be attributed to a cell stress relaxation as previously reported[40],[41]. It can be also noted that at all temperatures the cell volume is larger in the Yb-doped samples indicating the incorporation of Yb ions in the structural framework.

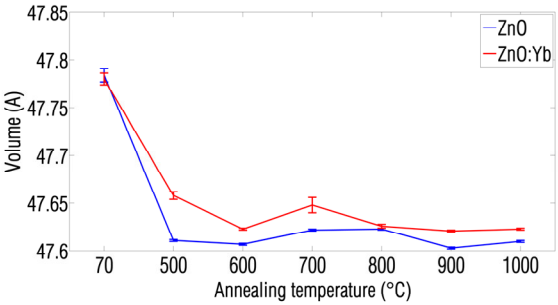

Figure 3 - Unit cell volume for pure ZnO and for doped ZnO:Yb-070 treated at different temperatures

However, at higher temperatures (≈800 °C), the cell volume of the doped sample presents a decreased value and a plateau or constant value that indicates the start of Yb_2O_3 segregation (Space group: Ia-3(206) - PDF 01-077-0453) as a pure phase, and the impoverishment of Yb in the doped phase[42]. The formation of this new phase is clearly observed in figure 4 through the appearance of the (222) Yb_2O_3 reflection in the XRD pattern of doped samples heated at 900 and 1000°C. A similar behavior was observed in[43] for ZnO doped with Er below 2%.

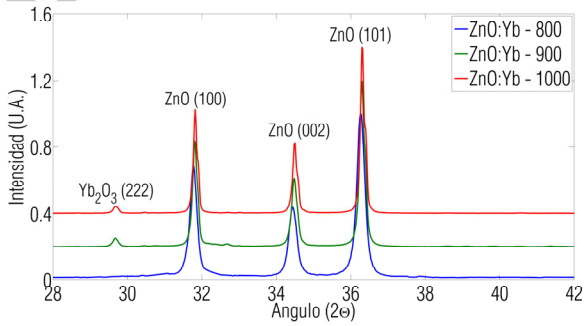

Figure 4 – XRD patterns of sample ZnO:Yb-070 treated at 800, 900 and 1000°C. The arrow indicates the segregated Yb_2O_3 phase

3.3 XAFS analysis

The XANES part of the XAFS spectra is a useful fingerprint for characterizing the absorbing atom environment. Figure 5a shows the XANES spectra at the Yb-L_3 edge of the as-prepared samples, ZnO:Yb-070, Yb_2O_3 and the metal organic precursor, $Yb(AcO)_3$. The spectra comparison indicates that the environment around the Yb atom in the sample differs from the oxides and the precursor.

Figure 5b shows the spectra of Yb_2O_3, and ZnO:Yb-070 samples heated at different temperatures. The environment of the Yb atom in samples ZnO:Yb-500 to ZnO:Yb-800 differs from that of Yb_2O_3. Samples treated at higher temperature exhibit similar spectra to Yb_2O_3, suggesting a similar environment for Yb atoms for these samples. This fact confirms the appearance of the sesquioxide, in accordance with the XRD analysis.

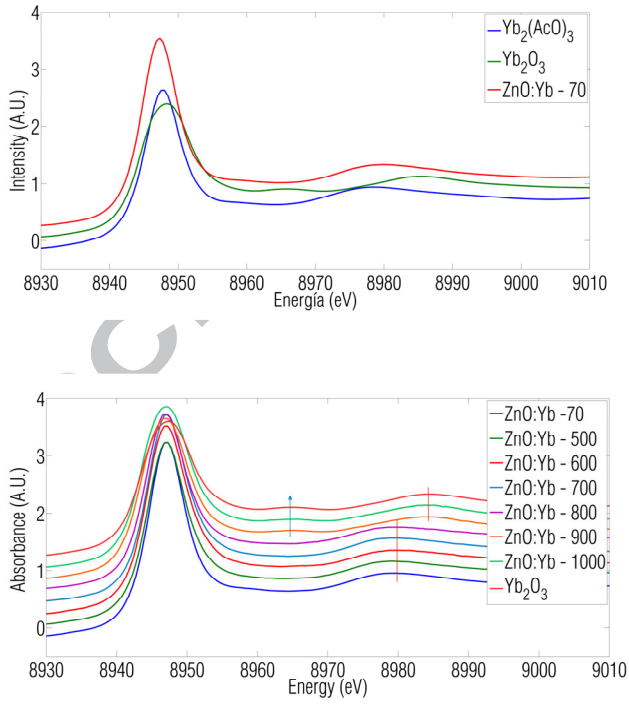

Figure 5 – Comparison of the XANES spectra at the Yb L_3-edge for ZnO:Yb-70 samples and the acetate precursor (Figure 5a)); and for ZnO:Yb-70 sample heated at different temperatures (Figure 5b)). The corresponding sesquioxide is also shown. Blue arrow and red lines indicate the difference among the spectra due to the thermal treatment. The spectra are vertically shifted to help visualization.

The Yb_2O_3 EXAFS spectra is shown in Figure 6 together with the ZnO:Yb-070 spectra treated at different temperatures. ZnO:Yb-070 sample only exhibits a first coordination shell, which may be attributed to a disordered environment at further distance according to Incoccia et al.[44].

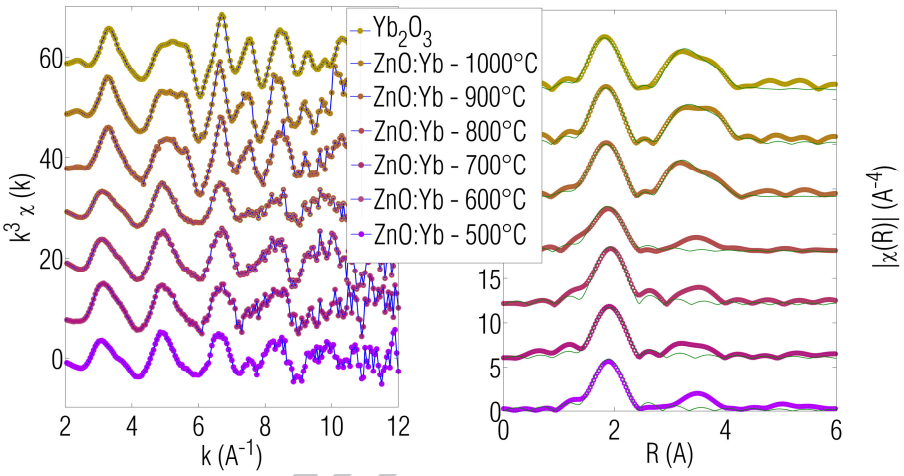

Figure 6 – *Left*: EXAFS region at the Yb L_3 edge for ZnO:Yb without thermal treatment, different thermal treatment (500-1000°C) and Yb_2O_3. *Right*: the corresponding fourier transform that gives information of the radial distribution of atoms around the absorbing atom. The fitting in R-space (blue line) was performed for the first coordination shell for all samples (table 3). The second coordination shell was performed only for ZnO:Yb - 900, ZnO:Yb - 1000 and Yb_2O_3. In the case of ZnO:Yb - 500 to ZnO:Yb - 800 there is a second shell that indicates an increased local order, but the data quality was not good enough to perform a fitting.

In table 3 (see Supporting Information), the results of the first coordination shell fitting are presented. The low dopant concentration in the samples and the low atomic weight of the backscattering atoms make difficult the structural parameters determination, exhibiting very low accuracy[44], [45]. The coordination number (CN) for the first shell is around 6 for all samples. In

the case of samples without treatment, the distance is bigger than in those thermally treated; this indicates that thermal annealing has an influence in the positioning of the lanthanide. For samples treated between 500°C and 800°C, the Yb-O distance is 2.31Å. This coincides with a possible location of Yb in an Oh interstitial position of ZnO lattice, where the distance between axial oxygen is 4,60Å. This result and the CNs numbers from table 3, indicate the existence of YbO_6, possibly located in interstitial positions of ZnO host.

The Radial Function Distribution (RFD) of ZnO:Yb-500 to ZnO:Yb-800 samples clearly show a second coordination shell. This remarkable fact indicates an increase of the local order in the Yb environment with thermal annealing. The fitting of the second coordination shell was impossible to perform due to the noisy signal, as a result of a low concentration of the absorbing atom. Also, as observed in the XANES spectra and XRD patterns, those samples treated at 900 and 1000°C present Yb_2O_3 phase segregation.

In order to determine the identity of the second coordination shell, we have applied the Continuous Cauchy Wavelet Analysis (CCWT) to the k^3-weighted EXAFS spectra, as the CCWT has proved to be a very useful tool to obtain structural information from complex systems. The EXAFS spectra can be visualized in a three dimensional graph: the wavevector (k), the radial function distribution without phase correction (R) and the modulus of the wavelet transform. The position in k-space is proportional to the backscattering factor, so atoms with different Z number will appear at different position in the k-space. Due to the large difference in Z values among O (Z=8), Zn (Z=30) and Yb (Z=70), the CCWT analysis easily differentiates the nature of the atoms present in the sample.

FEFF paths were generated and summed with ARTHEMIS and the CCWT was applied. The results were compared with the CCWT of the experimental data (Figure 7a). The result most similar to the experimental one was obtained with a combination of a first coordination shell

around 2,3Å composed by oxygen atoms and the second around 3.8Å composed by Zn atoms (Figure 7b). A simulation of a second shell composed by Yb atoms is also shown in Figure 7c, as clearly observed, the heavier atom, Yb, appears at higher frequencies than Zn. This result and the CNs numbers from table 3, indicate the existence of YbO_6 surrounded by Zn atoms and the inexistence of Yb_2O_3 clusters in the host lattice.

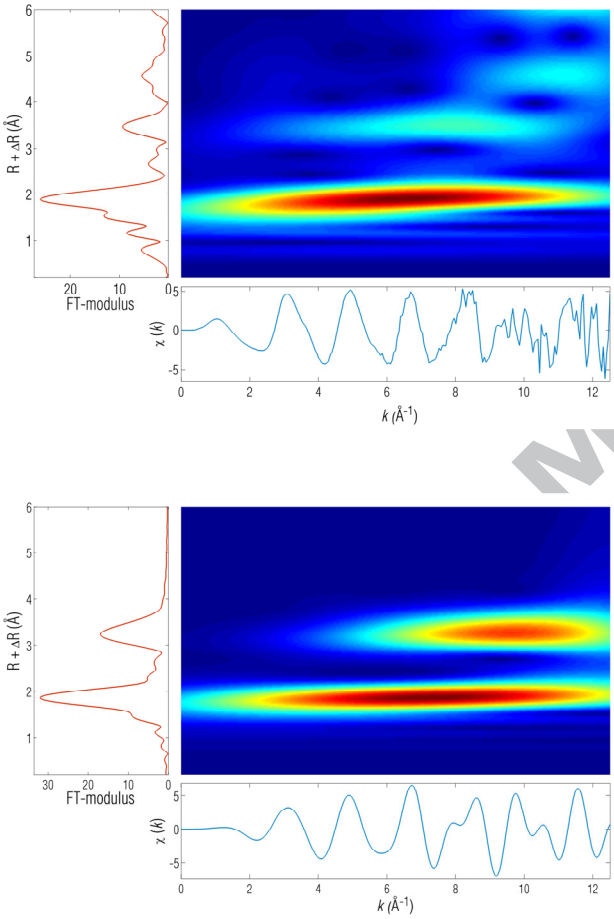

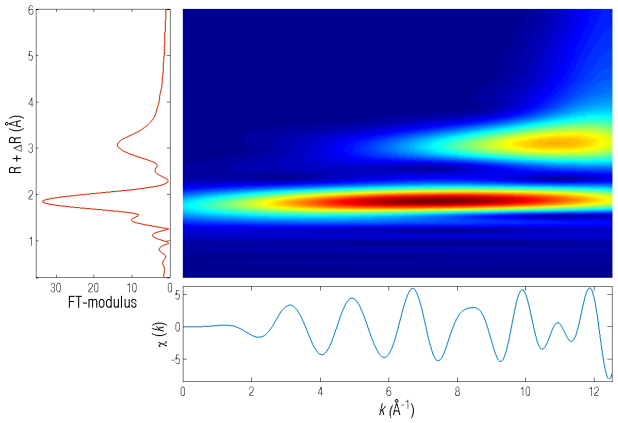

Figure 7 – Continuous wavelet analysis of A) experimental ZnO:Yb – 700, B) simulated FEFF paths of a first coordination shell composed by oxygen atoms and a second one composed by zinc atoms, C) Idem. but a second coordination shell is now composed by Yb atoms.

Figure 8 exhibits the postulated position of Yb atoms in the ideal ZnO wurtzite structure. According to the postulated position of Yb atoms, the EXAFS signal should exhibit Zn atoms at 1.9Å, but no signal is observed for Zn atoms at this distance. These Zn vacancies can be explained due to the need of charge balance in the lattice. The introduction of two Yb atoms in interstitial position will introduce positive charges that should be compensated with Zn vacancies, this mechanism can be expressed using the Kröger-Vink-Notation: $0 = 2Yb_i^{\bullet\bullet\bullet} + 3V_{Zn}^{''}$.

The presence of correlated Yb atoms was not detected in the measured range. In fact, this correlations are more easily observed in higher k ranges, k>10 $Å^{-1}$, where only the heavy atoms in the matrix contribute to the EXAFS signal[45]. Observation of this range of k should be performed in the Yb K edge due to the proximity of Zn K edge (9659eV).

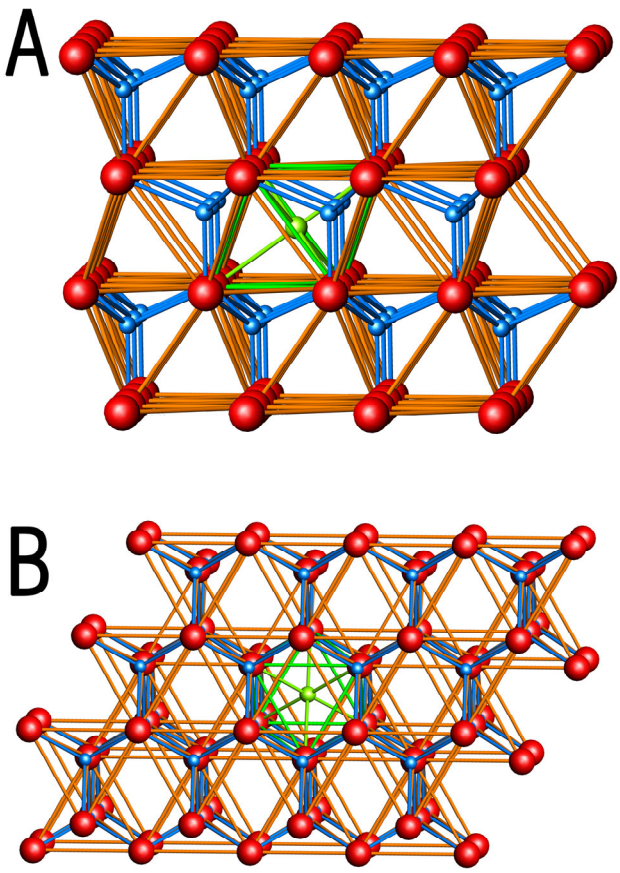

Figure 8 – Scheme of Yb atoms in ZnO lattice. A) along c-axis, B) along b-axis. The atoms in red, blue and green correspond to oxygen, zinc and ytterbium respectively.

The structural information obtained shows that the optimal thermal annealing for ZnO:Yb preparation is between 500 and 800°C, higher temperatures produce the phase segregation of the sesquioxide from the wurtzite host. Due to this fact, the system can be considered thermodynamically unstable at high temperatures, like all the nanostructured systems.

During the thermal treatment, the system suffers atomic rearrangement and the direct consequence of this atomic reconstruction is the reduction of imperfections in the lattice[46]. Hynes et al. have studied the dependence of the onset for this process during the sintering of ZnO, Al_2O_3 and Y_2O_3. They found that, as a rule of thumb, the required temperature for the sintering of a solid is a

fraction of the melting point (Tm): 0.8 – 0.9 Tm, but in case of nanocrystalline materials[47], this value may be decreased to 0.4 - 0.5 Tm.

The segregation of the lanthanides from the wurtzite structure can be attributed to a thermally activated mass transport and an atomic rearrangement. The mass transport drives the system to a more thermodynamically stable state by the segregation of the sesquioxide from the ZnO host. In the case of nanometric systems, these processes that usually take place at a temperature close to the melting point can be observed at lower temperatures because of the nanometric dimension of the solids.

In our case, the melting point of ZnO is 2248 K and the Yb_2O_3 segregation occurs in the range 1073-1173K (or 800-900°C), which approximately coincides with 0.5 Tm and with the onset for the sintering of a nanocrystalline system.

4. CONCLUSIONS

ZnO:Yb with good crystallinity and free of crystalline impurities were synthesized by a soft chemistry route and structurally characterized by X-ray techniques. The combined utilization of Rietveld refinement, XAS characterization and data analysis techniques proves the insertion of lanthanide ions in the O_h sites of the ZnO structure without phase segregation. Differently from our previous paper using XRD[43], where only the interstitial insertion could be postulated. The CCWT proved that the second coordination shell is composed of Zn atoms, confirming that the Yb atoms are incorporated in the structure without forming Yb_2O_3 clusters. The optimal range for thermal annealing of the obtained samples showed to be between 500°C to 800°C, higher temperatures showed Yb_2O_3 phase segregation. The reason for the segregation of the sesquioxide phase can be attributed to the mass transport and atomic rearrangement during the sintering of the nanopowders, which has its onset at lower temperature, 0.5 of Tm instead of 0.9 of a micrometric

system, because of the nanometric dimensions of the system.

AUTHOR INFORMATION

Corresponding Authors

* Tel: (54) 11 4709 8100 ext 1145. E-mail: eugenio.otal@citedef.gob.ar

ACKNOWLEDGMENTS

This work was financially supported by the YPF foundation (José A. Estenssoro PhD Grant), CONICET (Type 2 PhD Grant) and CITEDEF. The authors are grateful for being given access to the facilities of the XAFS (D04B - XAFS1 #6673, #7732 and #8239) beamlines at the LNLS. Also to Dr. Gustavo Azevedo from LNLS for his invaluable help in the XAFS measurements, Raul Tarulla from CITEDEF for ICP-EOS analysis and Matias Jobbágy from INQUIMAE-FCEN-UBA for the generous help in the thermal analysis of precursors.

SUPPORTING INFORMATION AVAILABLE:

Tables with refined crystal structure parameters for ZnO and ZnO:Yb and fitting results for the first coordination shell of ZnO:Yb samples treated at different temperatures. Intensity profile as a function of scattering angle and chi(k) as a function of energy.

REFERENCES

[1] D.A. Schwartz, N.S. Norberg, Q.P. Nguyen, J.M. Parker, D.R. Gamelin, Magnetic Quantum Dots: Synthesis, Spectroscopy, and Magnetism of Co2+- and Ni2+-Doped ZnO Nanocrystals, Journal of the American Chemical Society, 125 (2003) 13205-13218.
[2] E.H. Otal, M. Granada, H.E. Troiani, H. Cánepa, N.E. Walsöe de Reca, Nanostructured Colloidal Crystals from Forced Hydrolysis Methods, Langmuir, 25 (2009) 9051-9056.
[3] B. Liu, H.C. Zeng, Hydrothermal Synthesis of ZnO Nanorods in the Diameter Regime of 50 nm, Journal of the American Chemical Society, 125 (2003) 4430-4431.

[4] A.B. Hartanto, X. Ning, Y. Nakata, T. Okada, Growth mechanism of ZnO nanorods from nanoparticles formed in a laser ablation plume, Appl Phys A, 78 (2004) 299-301.
[5] Y. Tang, J. Chen, D. Greiner, L. Aé, R. Baier, J. Lehmann, S. Sadewasser, M.C. Lux-Steiner, Fast Growth of High Work Function and High-Quality ZnO Nanorods from an Aqueous Solution, The Journal of Physical Chemistry C, 115 (2011) 5239-5243.
[6] Y. Wang, X. Li, G. Lu, X. Quan, G. Chen, Highly Oriented 1-D ZnO Nanorod Arrays on Zinc Foil: Direct Growth from Substrate, Optical Properties and Photocatalytic Activities, The Journal of Physical Chemistry C, 112 (2008) 7332-7336.
[7] M.H. Huang, S. Mao, H. Feick, H. Yan, Y. Wu, H. Kind, E. Weber, R. Russo, P. Yang, Room-Temperature Ultraviolet Nanowire Nanolasers, Science, 292 (2001) 1897-1899.
[8] L.-Y. Chen, Y.-T. Yin, C.-H. Chen, J.-W. Chiou, Influence of Polyethyleneimine and Ammonium on the Growth of ZnO Nanowires by Hydrothermal Method, The Journal of Physical Chemistry C, 115 (2011) 20913-20919.
[9] D. Wang, G. Xing, M. Gao, L. Yang, J. Yang, T. Wu, Defects-Mediated Energy Transfer in Red-Light-Emitting Eu-Doped ZnO Nanowire Arrays, The Journal of Physical Chemistry C, 115 (2011) 22729-22735.
[10] Y. Dai, Y. Zhang, Q.K. Li, C.W. Nan, Synthesis and optical properties of tetrapod-like zinc oxide nanorods, Chemical Physics Letters, 358 (2002) 83-86.
[11] G. Malandrino, M. Blandino, M.E. Fragala, M. Losurdo, G. Bruno, Relationship between Nanostructure and Optical Properties of ZnO Thin Films, The Journal of Physical Chemistry C, 112 (2008) 9595-9599.
[12] Z.R. Tian, J.A. Voigt, J. Liu, B. McKenzie, M.J. McDermott, M.A. Rodriguez, H. Konishi, H. Xu, Complex and oriented ZnO nanostructures, Nat Mater, 2 (2003) 821-826.
[13] Han, Wang, Jie, W.C.H. Choy, Y. Luo, T.I. Yuk, J.G. Hou, Controllable Synthesis and Optical Properties of Novel ZnO Cone Arrays via Vapor Transport at Low Temperature, The Journal of Physical Chemistry B, 109 (2005) 2733-2738.
[14] N. Wang, X. Cao, Q. Wu, R. Zhang, L. Wang, P. Yin, L. Guo, Hexagonal ZnO Bipyramids: Synthesis, Morphological Evolution, and Optical Properties, The Journal of Physical Chemistry C, 113 (2009) 21471-21476.
[15] O. Lupan, B. Viana, T. Pauporté, M. Dhaouadi, F. Pellé, L. Devys, T. Gacoin, Controlled Mixed Violet–Blue–Red Electroluminescence from Eu:Nano-Phosphors/ZnO-Nanowires/p-GaN Light-Emitting Diodes, The Journal of Physical Chemistry C, 117 (2013) 26768-26775.
[16] K.S. Valeyev, V.A. Knayazev, N.G. Drozdov, elektrichestvo, 4 (1964) 72.
[17] M. Matsuoka, Nonohmic Properties of Zinc Oxide Ceramics, Japanese Journal of Applied Physics, 10 (1971) 736.
[18] Y. Sato, J.P. Buban, T. Mizoguchi, N. Shibata, M. Yodogawa, T. Yamamoto, Y. Ikuhara, Role of Pr Segregation in Acceptor-State Formation at ZnO Grain Boundaries, Physical Review Letters, 97 (2006) 106802.
[19] N. Jiang, S. Ye, J. Qiu, Electron energy-loss spectroscopy study of Yb doped ZnO, Journal of Applied Physics, 108 (2010) -.
[20] D.C. Kim, W.S. Han, B.H. Kong, H.K. Cho, C.H. Hong, Fabrication of the hybrid ZnO LED structure grown on p-type GaN by metal organic chemical vapor deposition, Physica B: Condensed Matter, 401–402 (2007) 386-390.
[21] X.-M. Zhang, M.-Y. Lu, Y. Zhang, L.-J. Chen, Z.L. Wang, Fabrication of a High-Brightness Blue-Light-Emitting Diode Using a ZnO-Nanowire Array Grown on p-GaN Thin Film, Advanced Materials, 21 (2009) 2767-2770.
[22] S. Bachir, J. Kossanyi, C. Sandouly, P. Valat, J.C. Ronfard-Haret, Electroluminescence of Dy3+ and Sm3+ ions in polycrystalline semiconducting zinc oxide, The Journal of Physical Chemistry, 99 (1995) 5674-5679.
[23] S. Ji, L. Yin, G. Liu, L. Zhang, C. Ye, Synthesis of Rare Earth Ions-Doped ZnO Nanostructures with Efficient Host−Guest Energy Transfer, The Journal of Physical Chemistry C, 113 (2009) 16439-16444.

[24] M. Abdullah, T. Morimoto, K. Okuyama, Generating Blue and Red Luminescence from ZnO/Poly(ethylene glycol) Nanocomposites Prepared Using an In-Situ Method, Advanced Functional Materials, 13 (2003) 800-804.
[25] L. Armelao, F. Heigl, A. Jürgensen, R.I.R. Blyth, T. Regier, X.T. Zhou, T.K. Sham, X-ray Excited Optical Luminescence Studies of ZnO and Eu-Doped ZnO Nanostructures, The Journal of Physical Chemistry C, 111 (2007) 10194-10200.
[26] S. Bachir, K. Azuma, J. Kossanyi, P. Valat, J.C. Ronfard-Haret, Photoluminescence of polycrystalline zinc oxide co-activated with trivalent rare earth ions and lithium. Insertion of rare-earth ions into zinc oxide, Journal of Luminescence, 75 (1997) 35-49.
[27] H.L. Han, L.W. Yang, Y.X. Liu, Y.Y. Zhang, Q.B. Yang, Up-conversion luminescence switching in Er3+-containing ZnO nanoparticles through Li+ co-doping, Optical Materials, 31 (2008) 338-341.
[28] Y.-P. Du, Y.-W. Zhang, L.-D. Sun, C.-H. Yan, Efficient Energy Transfer in Monodisperse Eu-Doped ZnO Nanocrystals Synthesized from Metal Acetylacetonates in High-Boiling Solvents, The Journal of Physical Chemistry C, 112 (2008) 12234-12241.
[29] E.A. Stern, D.E. Sayers, F.W. Lytle, Extended x-ray-absorption fine-structure technique. III. Determination of physical parameters, Physical Review B, 11 (1975) 4836-4846.
[30] M. Muñoz, P. Argoul, F. Farges, Continuous Cauchy wavelet transform analyses of EXAFS spectra: A qualitative approach, American Mineralogist, 88 (2003) 694-700.
[31] H. Funke, M. Chukalina, A.C. Scheinost, A new FEFF-based wavelet for EXAFS data analysis, Journal of Synchrotron Radiation, 14 (2007) 426-432.
[32] J. Timoshenko, A. Kuzmin, Wavelet data analysis of EXAFS spectra, Computer Physics Communications, 180 (2009) 920-925.
[33] H. Funke, A.C. Scheinost, M. Chukalina, Wavelet analysis of extended x-ray absorption fine structure data, Physical Review B, 71 (2005) 094110.
[34] M. Sahnoun, C. Daul, O. Haas, Wavelet investigation of La0.5Ca0.5CoO3−δ x-ray absorption data, Journal of Applied Physics, 101 (2007) -.
[35] R.O. Savinelli, S.L. Scott, Wavelet transform EXAFS analysis of mono- and dimolybdate model compounds and a Mo/HZSM-5 dehydroaromatization catalyst, Physical Chemistry Chemical Physics, 12 (2010) 5660-5667.
[36] M. Muñoz, F. Farges, P. Argoul, Continuous Cauchy wavelet transform of XAFS spectra, Physica Scripta, 2005 (2005) 221.
[37] B. Toby, EXPGUI, a graphical user interface for GSAS, Journal of Applied Crystallography, 34 (2001) 210-213.
[38] P. Stephens, Phenomenological model of anisotropic peak broadening in powder diffraction, Journal of Applied Crystallography, 32 (1999) 281-289.
[39] B. Ravel, M. Newville, ATHENA, ARTEMIS, HEPHAESTUS: data analysis for X-ray absorption spectroscopy using IFEFFIT, Journal of Synchrotron Radiation, 12 (2005) 537-541.
[40] H.K. Kim, M. Mathur, Thermally stable ZnO films deposited on GaAs substrates with a SiO2 thin buffer layer, Applied Physics Letters, 61 (1992) 2524-2526.
[41] N. Salah, S.S. Habib, A. Memic, A. Azam, E. Alarfaj, N. Zahed, S. Al-Hamedi, High- Energy Ball Milling Technique for ZnO Nanoparticles as Antibacterial Material, Int. J. nanomed., 6 (2011) 863-869.
[42] L. Armelao, G. Bottaro, M. Pascolini, M. Sessolo, E. Tondello, M. Bettinelli, A. Speghini, Structure−Luminescence Correlations in Europium-Doped Sol−Gel ZnO Nanopowders, The Journal of Physical Chemistry C, 112 (2008) 4049-4054.
[43] E.H. Otal, S. Yoon, M. Aguirre, A. Weidenkaff, Metastability of heavy lanthanides in the ZnO wurtzite structure, Journal of Alloys and Compounds, 509, Supplement 1 (2011) S364-S366.
[44] L. Incoccia, S. Mobilio, Debye-Waller Factors in R-Space Analysis, in: A. Bianconi, L. Incoccia, S. Stipcich (Eds.) EXAFS and Near Edge Structure, Springer Berlin Heidelberg, 1983, pp. 91-95.
[45] F. d'Acapito, R. Francini, S. Pietrantoni, D. Barbier, The Site of Er in Phosphate Glasses Studied by K-Edge EXAFS, AIP Conference Proceedings, 882 (2007) 401-403.
[46] J. Philibert, Atom Movements: Diffusion and Mass Transport in Solids, Editions de Physique, 1991.

[47] A.P. Hynes, R.H. Doremus, R.W. Siegel, Sintering and Characterization of Nanophase Zinc Oxide, Journal of the American Ceramic Society, 85 (2002) 1979-1987.

Optical and electrical properties of ZnO are influenced by lanthanides doping.

Optical and electrical properties of ZnO are influenced by lanthanides positioning.

Yb is incorporated in the Oh sites of the wurtzite structure.

There is not Yb_2O_3 clustering or segregation for treatments below 800°C.